Rapid Estimation of Fault Parameters for Tsunami Warning along the Mexican Subduction Zone: A Scenario Earthquake in the Guerrero Seismic Gap

by Xyoli Pérez-Campos, Diego Melgar, Shri K. Singh, Víctor Cruz-Atienza, Arturo Iglesias, and Vala Hjörleifsdóttir

Online Material: To be sent later.

INTRODUCTION

The devastating tsunami produced by the Sumatra–Andaman earthquake (M_w 9.2) of 24 December 2004 heightened the interest of the scientific community in tsunami early warning system. Global efforts have been successful in achieving a robust ocean basin-wide tsunami warning in which there is enough time to obtain accurate source parameters, determine the tsunami potential, model the tsunami propagation through the oceans, and update it with real-time sea-surface height observations. However, local systems are still not reliable. In such cases, rapid estimation of accurate source parameters that are expeditious in discriminating a tsunamigenic earthquake and its potential tsunami are essential. The 2011 Tohoku–Oki earthquake (M_w 9.0) revealed that tsunami-warning techniques based on traditional seismic instrumentation could lead to an underestimation of the event magnitude (Ozaki, 2011), which can translate into tragic loss of life and infrastructure (e.g., Cyranosky, 2011).

The Pacific coast of Mexico has been struck by at least 26 historic tsunamis originating from local subduction earthquakes (Sánchez and Farreras, 1993; Farreras, 1997). Tide-gauge recording in Mexico began in 1952. Since then, the maximum height recorded is 3 m for the 1985 Michoacán earthquake (M_w 8.0). However, historic documents suggest that tsunamis as high as 8–11 m may have hit the Mexican Pacific coast during the Guerrero–Oaxaca earthquake of 28 March 1787, M_w 8.4–8.6 (Sánchez and Farreras, 1993; Farreras, 1997; Núñez-Cornú *et al.*, 2008; Suárez and Albini, 2009) and the Colima–Jalisco earthquake of 22 June 1932, M_w 7.0 (Sánchez and Farreras, 1993; Farreras, 1997). An effective tsunami early warning system for the Mexican Pacific coast should be able to emit a reliable alert in less than 10 minutes, given that the peak in the tsunami height may reach the coast about 10–15 minutes after the origin time of the earthquake (M. Ortiz, personal comm., 2007).

Following the 1985 Michoacán earthquake, great interest has been focused on the Guerrero segment of the Mexican subduction zone, which had previously been identified as a seismic gap (Singh *et al.*, 1980, 1981, 1982; Anderson *et al.*, 1989; Suárez *et al.*, 1990; Fig. 1, Ⓔ supplement). The proximity of the Guerrero coast to Mexico City, compared with the more distant Michoacán coast, intensified concern among scientists and authorities. As a result, a seismic early warning system was conceived and deployed for Mexico City, which has monitored the Guerrero seismic gap since 1991 (Espinosa-Aranda and Rodríguez, 2003). However, the observational goal of the system is early warning of an earthquake with an epicenter within the Guerrero seismic gap and to issue a warning solely to Mexico City. Kanamori *et al.* (1993) and Ordaz *et al.* (1995) both simulated strong ground motions in Mexico City for postulated M_w 8.0 and 8.1 earthquakes in the Guerrero seismic gap, respectively. These simulations were two to three times as large as the one produced by the 1985 Michoacán earthquake.

In an effort to test our scientific preparedness and develop effective warning tools, a group of seismologists at the Institute of Geophysics at the Universidad Nacional Autónoma de México (UNAM) launched a scenario earthquake in the Guerrero seismic gap. The test was a blind one; the source parameters were unknown to the analysis team and were revealed only after all the tests were performed. This paper is focused on a rapid assessment of the source parameters and the tsunamigenic potential of the scenario earthquake. The objective is to test an algorithm we have developed that relies on a method described in Singh *et al.* (2012) based on real-time to near real-time estimates of the static-displacement field (ideally measured from a Global Positioning System [GPS]).

We analyze synthetic-displacement time series generated for this scenario earthquake to determine the time it will take to obtain robust source-parameter estimates and assess the

doi: 10.1785/0220120156

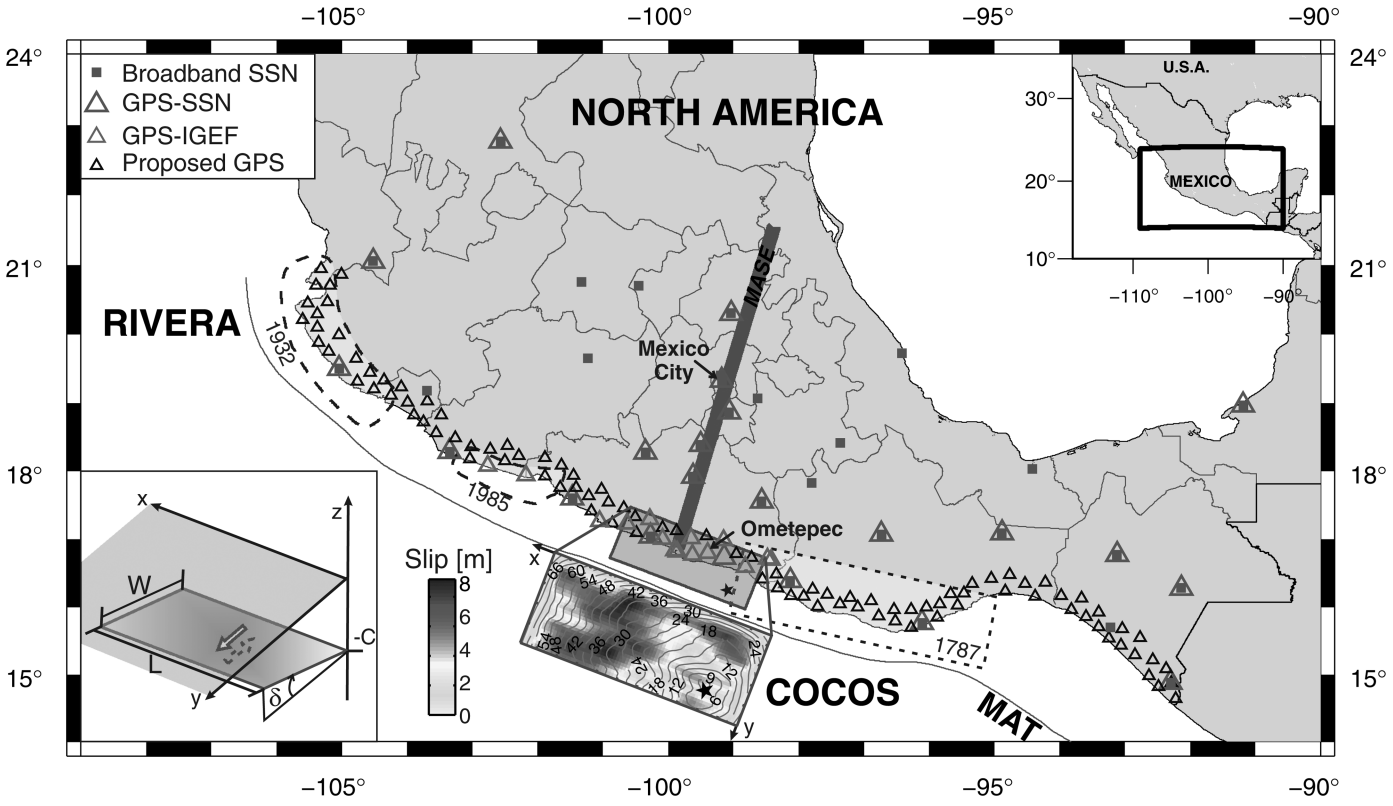

▲ **Figure 1.** Guerrero rupture scenario, broadband seismic network and GPS station locations. Rupture areas for historic earthquakes ($M_w \geq 8$) are denoted by the elongated dashed shapes. The rupture area for the 1787, the 1932, and the 1985 earthquakes are taken from Suárez and Albini (2009), Singh, Ponce, and Nishenko (1985), and UNAM Seismology Group (1986), respectively. The location of the Meso American Subduction Experiment (MASE) profile is shown as a thick gray line. The rupture area used by Cruz-Atienza *et al.* (2011) for the scenario earthquake is shown as a dark gray rectangle, the slip on the fault is in meters and rupture time contours in seconds, the black star denotes the epicenter. Middle America Trench (MAT); Servicio Sismológico Nacional (SSN); GPS network operated by the SSN (GPS–SSN) with real-time transmission capacity of 1 sample per second; autonomous GPS stations operated by individual researchers or groups from the Instituto de Geofísica, UNAM (GPS–IGEF). Geometry from Okada (1992) is in the lower corner: L and W are the length and the width of the fault, respectively, δ is the dip and $-C$ is the depth of the downdip edge of the fault. x and y axes are oriented along and perpendicular to the coast (towards to the trench), respectively. For coastal GPS stations $y \approx 0$.

uncertainty in the parameters, given the GPS network configuration. We also estimate the focal mechanism from a W-phase inversion of synthetic seismograms calculated for the Servicio Sismológico Nacional (SSN) broadband stations. As we will see, a tsunami warning would have been issued for this scenario earthquake from the estimated magnitude in about two minutes. We would also have correctly estimated the length of the rupture and surface projection of the downdip edge of the fault with respect to the coast. The knowledge of the location of the downdip edge is important because a large earthquake with a rupture area that lies partly below the continent may have relatively enhanced high-frequency radiation and generate severe ground motions, thus causing damage to engineering structures and loss of life. On the other hand, if the rupture area lies mostly offshore, then the high-frequency radiation may be relatively depleted and the earthquake may not produce large, destructive ground motions. However, it may have a higher tsunamigenic potential because a larger area of sea floor will experience vertical motion.

There is an urgent need for a denser GPS network and real-time tracking of the position of GPS sites along the Pacific coast of Mexico. This need is emphasized by the recent Ometepec earthquake of 20 March 2012 (M_w 7.4) that occurred south of the Guerrero gap. In this instance, there was only one real-time GPS station in the epicentral zone. There are a few GPS sites in and near the epicentral area in which data are presently obtained in campaign mode. Had these data been available in real time, a correct M_w would have been obtained, but the length of the rupture would have been overestimated due to an inadequate number of stations.

SCENARIO EARTHQUAKE AND SYNTHETIC DISPLACEMENT DATA

An M_w 8.2 earthquake was proposed as the scenario event to fill the entire Guerrero seismic gap. This gap extends from the southern edge of the two Michoacán 1985 earthquakes up to the Ometepec region (Fig. 1, Ⓔ supplement). Based on the

magnitude and geometry of the slab in this region, Cruz-Atienza *et al.* (2011) generated a kinematic slip distribution and rupture propagation on a 210×90 km^2 fault with strike $\phi_s = 292°$, dip $\delta = 13°$, and rake $\lambda = 90°$. Following Mai and Beroza (2002), the final slip distribution was stochastically generated using a spatial random field modulated by a von Karman autocorrelation function for which the correlation lengths increase with source dimension. Local rupture velocities (i.e., source rupture times) were determined as a function of local final slips with respect to a mean value of 2.8 km/s. Slip-rate time histories are the dynamic-rupture consistent functionals originally introduced by Yoffe (1951) and then regularized by Tinti *et al.* (2005). The hypocenter was at 16.513° N, 99.859° W, at 7 km depth. The average slip on the fault is 4.1 m with a maximum of 9.2 m to the northeast of the hypocenter. The overall fault parameters are listed in Table 1.

Synthetic seismograms Ⓔ (supplement) were generated at current SSN station locations within a region of 1200 km along the coast and 700 km inland (Cruz-Atienza *et al.*, 2011) by mean of a parallel-finite difference code (Olsen *et al.*, 2009) running on the Pohualli supercomputer of the Departamento de Sismología at UNAM. The shear-wave velocity model was taken from Iglesias *et al.* (2010). This model was obtained along the profile of the MesoAmerican Subduction Experiment (MASE; Fig. 1, Ⓔ supplement), oriented perpendicular to the coast and included the slab with the geometry inferred from receiver functions and tomography (Pérez-Campos *et al.*, 2008). This model was then projected laterally to generate a 2.5D model. The quality factors were taken as follows: $Q_S = 50V_S$, and $Q_P = 2Q_S$.

For our tests, we utilized displacements time series generated at 22 GPS stations and velocity seismograms at 24 broadband seismic stations (Fig. 1, Ⓔ supplement). The 22 GPS stations correspond to 6 stations located along the Pacific coast operated by the SSN and 16 coastal stations operated by Instituto de Geofísica, UNAM. The SSN stations are currently transmitting 1 Hz data in real time to Mexico City. The other 16 stations operate autonomously at 1 Hz and the data is collected on a regular basis or as soon as possible after the occurrence of an interesting event. Broadband seismic stations are part of the SSN network. All of the SSN GPS stations are colocated with broadband (STS-2) and strong motion (FBA-23) sensors.

REAL-TIME SOURCE PARAMETER ESTIMATION

Singh *et al.* (2008) proposed a method for rapid and robust determination of fault parameters of subduction earthquakes based on Okada's (1992) model (inset Fig. 1, Ⓔ supplement) as follows: length of the fault L, average displacement on the fault D, and position of the fault, in particular the relative position of the surface projection of its downdip edge with respect to the coast, c. Needed critical parameters of most, if not all, seismogenic zones (width W_s, strike ϕ_s, dip δ, rake λ, and maximum depth of the downdip edge, C) are known from previous studies and static coseismic displacements are obtained from coastal GPS stations. For large Mexican subduction earthquakes ($M_w > 7.6$), we take $W_s = 80$ km, $\phi_s = 292°$, $\delta = 15°$, $\lambda = 90°$, and $C = 25$ km (e.g., Chael and Stewart, 1981; Singh, Suárez and Domínguez, 1985; Suárez *et al.*, 1990; Singh and Mortera, 1991; Pacheco and Singh, 2010).

Singh *et al.* (2012) described the criteria for estimating L, D, and c. L is obtained from observed horizontal displacements perpendicular to the trench, U_y (Fig. 1, Ⓔ supplement). L is assumed to extend laterally up to the point where $U_y < 0.2(U_y)_{\max}$. In Okada's model, $y = 0$ corresponds to the surface projection of the fault's downdip edge so that $y = c$ defines the horizontal distance of the coast from the surface projection of the fault's downdip edge. c is determined from

Table 1
Input and Estimated Fault Parameters for Earthquake Scenarios

		Test 1 (6 Stations)		Test 2 (22 Stations)		Test 3 (93 Stations)	
Parameter	Scenario*	119†	290†	119†	290†	119†	290†
Number of stations		2	6	12	22	29	93
Strike, ϕ_s (°)	292	292‡		292‡		292‡	
Dip, δ (°)	13	15‡		15‡		15‡	
Rake, λ (°)	90	90‡		90‡		90‡	
Length, L (km)	210	341	311	204	206	175	204
Width, W (km)	90	80		80		80	
c (km)	37	41		39		38	
Average slip, D (cm)	406.6	506	506	592	592	555	534
M_0 ($\times 10^{21}$ N·m)		4.14	3.78	2.90	2.92	2.33	2.61
M_w	8.2	8.34	8.32	8.24	8.24	8.18	8.21

c is the distance from the surface projection of the downdip edge of the fault to the coast.
*From Cruz-Atienza *et al.* (2011).
†Seconds after origin time.
‡Assumed values for Mexican subduction earthquakes.

the observed vertical displacements, U_z. Given the geometry of the fault ($\delta = 15°$ and $C = 25$ km), the projection of the fault's downdip edge is 13 km inland from the point where U_z changes sign. If no change on the sign is observed and all the values of U_z are positive, the projection of the downdip edge of the fault will be assumed to be 13 km from the station farthest from the coast where $U_y \geq 0.2(U_y)_{\max}$. Otherwise, if all U_z are negative, the projection of the downdip edge of the fault will be assumed to be 13 km towards the trench from the station closest to the coast with $U_y \geq 0.2(U_y)_{\max}$. D is then computed as the uniform slip on a rectangular fault that produces U_y equal to the observed average U_y, $\langle U_y \rangle$. The fault width W is taken equal to L if $L < W_s$ or equal to W_s if $L \geq W_s$.

Once L, D, and c are estimated, then the seismic moment M_0 and the moment magnitude M_w, are calculated as $M_0 = \mu LWD$ and $M_w = 2/3 \log M_0 - 6.07$ (M_0 in N·m), respectively. We assume $\mu = 3 \times 10^4$ MPa. Singh *et al.* (2012) successfully tested the method on nine large earthquakes (M_w 7.3–9.0), including the Tohoku–Oki 2011 mainshock and the Sumatra–Andaman 2004 earthquake and two earthquakes in Mexico, Colima–Jalisco 1995 and in Tecomán, Colima, 2003. The test by Singh *et al.* (2012) was performed using coseismic GPS static displacements reported in the literature; however, Singh *et al.* (2012) suggested that the method can be used in real time once the system detects displacement vectors exceeding a threshold level at more than a certain pre-established number of contiguous stations.

Following Singh *et al.* (2012), the algorithm consists of two initial steps: (1) to determine if a threshold has been exceeded by several contiguous GPS stations within a time window determined by the mean distance between stations, and (2) to estimate the M_w and fault location. These two parameters could trigger a first alert to be modified as other parameters become available. Because the focal mechanism plays an important role in tsunami generation, its rapid determination is desirable. Currently, a focal mechanism can be obtained within 2–5 minutes for regional earthquakes with a variety of methods such as W-phase inversion (e.g., Rivera *et al.*, 2011) or from the fastCMT GPS inversion (Melgar *et al.*, 2012). However, the W phase relies on an initial input for location and magnitude of the event and both the W phase and fastCMT methods are point-source inversions that run into problems with fault finiteness for large events. Here we test a W-phase inversion using as input parameters that were obtained in step 2.

For the determination of coseismic displacements at GPS stations along the coast from high-rate data, we follow Melgar *et al.* (2012). We calculate a 50 s window moving average at each time step, as well as the standard deviation on a 20 s window of the moving average (Fig. 2, Ⓔ supplement). If 20% is exceeded on the standard deviation of at least 2 contiguous stations, and this level is maintained for at least 20 s, the system will declare that an event has started. Coseismic slip is determined at each station when standard deviation has again been reduced by 20%. Because GPS data tends to be noisy, it is undesirable to rely on data from a single epoch. Thus, the value of the coseismic slip is computed from the mean of 10 samples after the trigger has been set. The sampling rate used is 1 Hz, sufficient for static offset computation. Higher sampling rates are recommended for full waveform analysis (Smalley, 2009; Avallone *et al.*, 2011; Bock *et al.*, 2011) although this is potentially very taxing on telemetry.

As coseismic displacement is being determined at each station, it is included into the fault-parameter estimation. Once the length of the fault shows no significant variation by adding more station information, the estimated fault parameters are established as input for the solution of the position of the fault and the M_w. Then, a hypocenter based on the estimated position of the fault and M_w are used to start the W-phase inversion for the focal mechanism. We use as the hypocenter the center of the rectangle estimated in step 2. Because we are only interested in a rough but quick estimate of the focal mechanism, no extra effort is expended in finding the best solution, such as a grid search for the duration of the moment-rate function or the position of the centroid.

RESULTS FOR THREE NETWORK CONFIGURATIONS

We test three network scenarios. The first scenario only includes GPS stations operated by the SSN that at present are the only ones with real-time transmission capability. This leaves us with only six stations along the Pacific coast (Fig. 2, Ⓔ supplement). The mean distance between the stations is 164 km. At minute 01:59 after the origin time (OT), two stations have detected the event, coseismic displacement has been calculated, fault parameters estimated and a $M_0 = 4.4 \times 10^{21}$ N·m (M_w 8.34) has been obtained. The position of the projection of the downdip edge of the fault with respect to the coast suggests that the rupture has extended inland.

The W-phase inversion is then triggered with a hypocenter location at 16.87° N, 99.77° W, and 15 km depth. Stations at distances between 1° and 4° are used for the inversion in order to have a quick solution. A first solution shows a reverse focal mechanism with a lower seismic moment of $M_0 = 1.53 \times 10^{21}$ N·m (M_w 8.06) (Table 2). At minute 4:50, all six GPS stations along the coast have detected the event, giving a $M_0 = 3.78 \times 10^{21}$ N·m (M_w 8.32). The W-phase inversion gives a shallow dip reverse mechanism with $M_0 = 1.19 \times 10^{21}$ N·m (M_w 7.98), with stations up to a distance of 6° (Table 2).

For the second test, we utilize the data from all the 22 GPS stations currently operating along the Pacific coast. The average distance between them is 41 km (Fig. 3, Ⓔ supplement). At minute 01:25 after the origin time, 3 stations have detected the event and we get a first estimate of $M_0 = 4.83 \times 10^{20}$ N·m (M_w 7.72). However, only 34 s later, 12 stations have detected the event and we obtain $M_0 = 2.90 \times 10^{21}$ N·m (M_w 8.24). There is no significant change after this moment. At minute 4:50, all 22 GPS stations along the coast have detected the event, giving a $M_0 = 2.92 \times 10^{21}$ N·m (M_w 8.24). W-phase

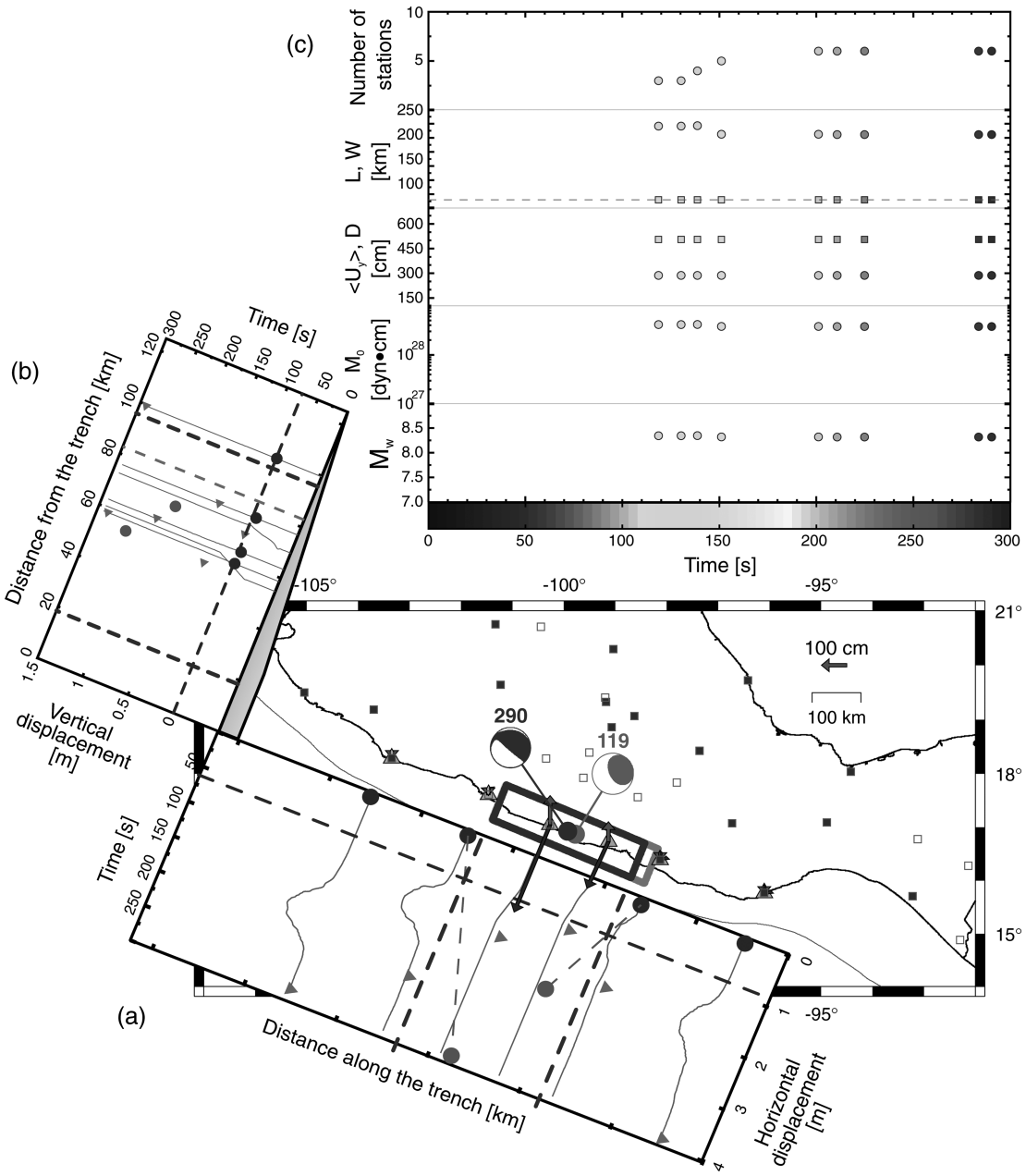

▲ **Figure 2.** Results from test 1. Fault parameters from GPS–SSN stations with real-time transmission capability and focal mechanism from *W*-phase inversion using regional broadband stations. The map shows the GPS stations as triangles, solid symbols for those that detected the event within three minutes. Broadband stations are denoted by squares and stations used in the *W*-phase inversion by solid symbols. Displacement vectors are shown for each station, dark gray for U_y (displacement perpendicular to the trench) and light gray for U_z (vertical displacement). Solid circles on the map, show the location of the epicenter used for the *W*-phase inversion (center of the fault), the gray shade corresponds to time: 119 s in light gray and 290 s in dark gray. The focal mechanisms show the results from the *W*-phase inversion at 119 s (light gray) and 290 s (dark gray). (a) Moving average of U_y with respect to time and with distance along the trench. Triangles show the time when the static-coseismic displacement is determined for each station. Solid circles represent the value of $U_y \geq (U_y)_{20}$ in light gray, and $U_y < (U_y)_{20}$ in dark gray. The dash line denotes $U_y = (U_y)_{20}$. Thin dashed lines denote delinear regression used to find the intercept with $U_y = (U_y)_{20}$ to establish the fault lateral limits denoted by the thick dashed lines. (b) Moving average of U_z with respect to time and with distance from the trench. Triangles show the time when the static-coseismic displacement is determined for each station. Solid circles represent the value of U_y, $U_y \geq (U_y)_{20}$ in light gray and $U_y < (U_y)_{20}$ in dark gray. The dash line denotes $U_z = 0$. The thin dashed line denotes the change from $U_z > 0$ to $U_z < 0$; the updip and downdip limits are denoted by the thick dashed lines. (c) Solutions with time. Each column of symbols corresponds to the solution obtained at that time. In the second row, circles correspond to *L* and squares to *W*; W_s is denoted by the dashed line. In the third row, circles correspond to $\langle U_y \rangle$ and squares to *D*.

Table 2
W*-Phase Inversion for Earthquake Scenarios

Parameter	True CMT*	Test 1 (6 Stations)		Test 2 (22 Stations)		Test 3 (93 Stations)	
		119†	290†	119†	290†	119†	290†
Latitude (°)	16.739	16.87‡	16.93‡	16.73‡	16.75‡	16.71‡	16.75‡
Longitude, (°)	−99.780	−99.77‡	−99.90‡	−99.64‡	−99.68‡	−99.62‡	−99.71‡
Num. stat., num chan.	—	10, 30	17, 51	11, 33	16, 48	12, 36	16, 48
Δ_{min}(°), Δ_{max} (°)	—	1.8, 3.7	1.8, 6.0	1.7, 3.9	1.9, 6.0	1.7, 3.9	1.9, 5.8
NP1, ϕ_s(°)/δ(°)/λ(°)	292/13/90	276/17/38	264/15/43	258/12/10	275/19/45	73/12/−145	275/20/45
NP2, ϕ_s(°)/δ(°)/λ(°)	—	149/80/104	132/80/101	159/88/102	141/77/104	309/83/−80	142/76/105
M_0(×10^{21} N·m)	2.48	1.53	1.19	2.01	2.02	2.84	1.78
M_w	8.2	8.06	7.98	8.14	8.14	8.24	8.13

*Depth was set to 15 km for the inversion; centroid depth was at 14.2 km.
†Seconds after origin time.
‡Position of the center of the rectangle assumed as centroid, this was used as input for the inversion.

inversion with data from stations at distances between 1° and 6° distance, gives a shallow dip reverse mechanism with $M_0 = 1.64 \times 10^{21}$ N·m (M_w 8.05; Table 2). This was assuming the hypocenter location at the center of the fault and at a depth of 15 km. The position of the projection of the downdip of the fault suggests that the fault has extended inland.

From the previous two tests, it is clear that in order to have a robust estimate in the shortest time possible (less than two minutes), a smaller distance between stations is required. Furthermore, for the first test we only have one row of stations parallel to the trench; therefore, if U_z were negative there would be no way to better constraint the position of the downdip edge of the rupture. We perform a third test based on an ideal network that consists of 120 stations of 2 parallel rows along the coast. It includes 22 stations currently in operation (Fig. 4, Ⓔ supplement). The mean distance between each station is 12.5 km. Because over-estimation of the magnitude can be as undesirable as under-estimation, the accuracy on the first estimate is important. Only 93 stations were inside of the simulation domain. At minute 01:27 after OT, three stations have detected the event and a first estimate of L is 175 km, c is 38 km (e.g., the projection of the downdip edge is 38 km from the coast), and $M_0 = 5.80 \times 10^{20}$ N·m (M_w 7.78). However, only 32 s later (i.e., 01:59 minutes after rupture initiation), 29 stations have already detected the event. L is estimated as 204 km, c remains the same and $M_0 = 2.33 \times 10^{21}$ N·m (M_w 8.18). There is no significant change after this point in time. At minute 4:50, 93 GPS stations along the coast have detected the event, giving a $M_0 = 2.61 \times 10^{21}$ N·m (M_w 8.21). In this ideal scenario, we would trigger the W-phase inversion when further lateral stations, two on each side, show $U_y < 0.2(U_y)_{max}$. The inversion, using as an epicenter the center of the fault previously determined and broadband stations between 1° and 6° distance, gives a shallow dip reverse mechanism with $M_0 = 1.97 \times 10^{21}$ N·m (M_w 8.13) (Table 2). This process takes an additional ~2 minutes. In other words, in less than five minutes, all the relevant source parameters, including the focal mechanism, would be available.

THE OMETEPEC EARTHQUAKE OF 2012

On 20 March 2012, an M_w 7.4 subduction earthquake took place south of the Guerrero seismic gap. The epicentral region is well known for similar events in the past (Astiz and Kanamori, 1984; Nava, 1984; Quintanar, 1985; Nishenko and Singh, 1987; Courboulex *et al.*, 1997).

Only one GPS station, PINO, operated by the SSN and transmitting 1 Hz data in real time, was located in the epicentral zone; the next 2 closest coastal stations operating in a similar mode were CAYA and HUAT, located more than 200 km from the epicenter (Fig. 5, Ⓔ supplement). Because of very sparse coastal GPS network along the coast, our algorithm has not as yet been implemented at SSN. For this reason, we only investigated whether the static-displacement field retrieved from autonomous (non-real-time) GPS stations in and near the epicentral area: OMTP, MRQL, and OXTU, along with PINO, CAYA, and HUAT (Fig. 5, Ⓔ supplement) would have yielded reasonable source parameters. For this station configuration, we obtain $L = 110$ km, $W = W_s = 80$ km, and $M_0 = 1.67 \times 10^{20}$ N·m (M_w 7.41). Given that both OMTP and PINO show a negative U_z, the downdip edge of the fault is set southwest of station PINO (Fig. 5, Ⓔ supplement). The length of the fault is still larger than expected from preliminary analysis of aftershocks and inversion of local and regional waveforms, which suggest a fault area of ~35 km × 35 km ((UNAM Seismology Group, 2013). Thus, L (and hence W) estimated from the static field is too large, which is undoubtedly a consequence of the large distance between stations. However, the estimated M_w is in excellent agreement with that obtained from the real-time regional W-phase inversion (M_w 7.43) and that reported by GCMT (M_w 7.5).

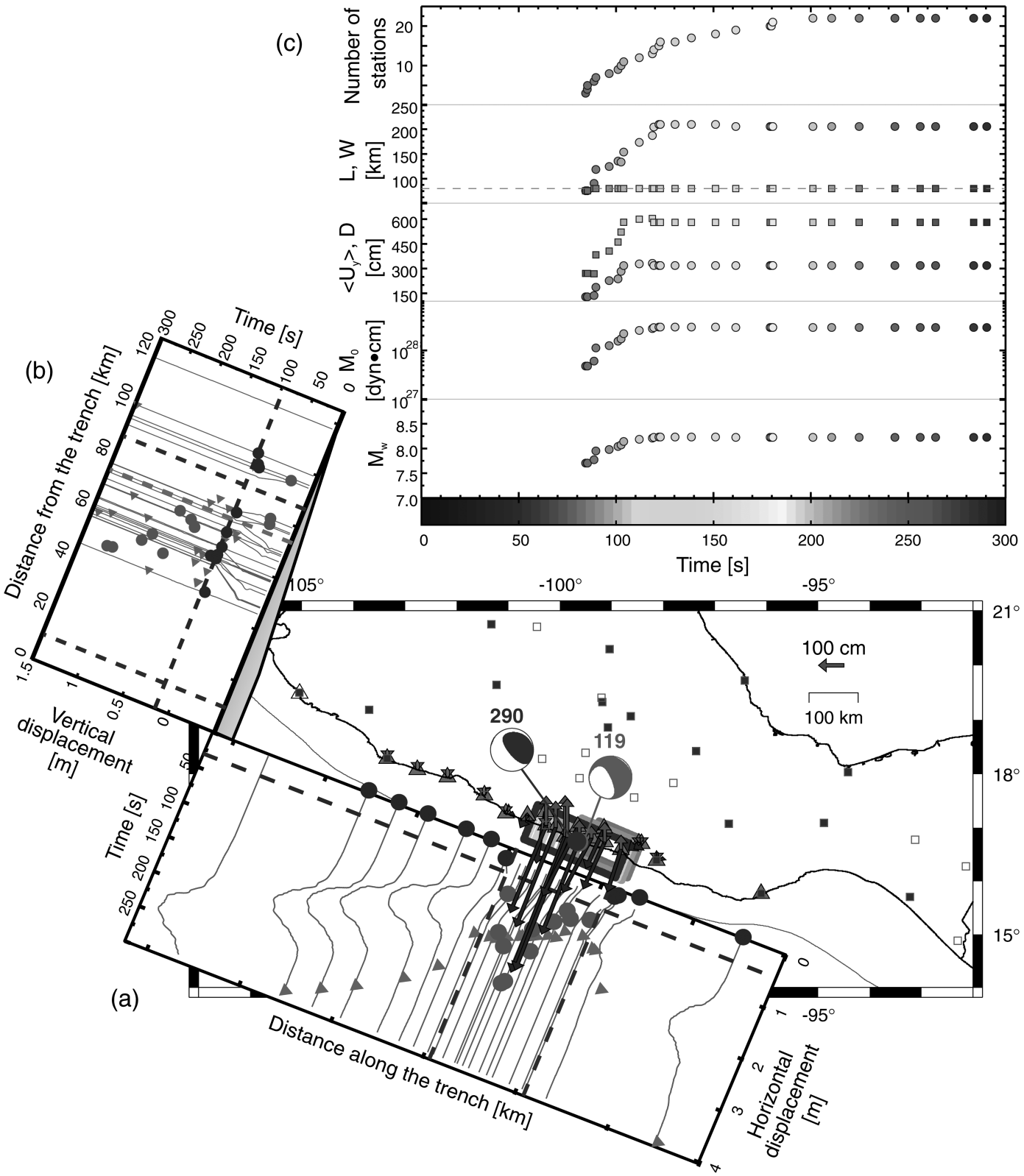

▲ **Figure 3.** Results from test 2. Fault parameters from the existing 22 GPS stations along the coast and focal mechanism from *W*-phase inversion using regional broadband stations. Symbols and panels are the same as for Figure 2.

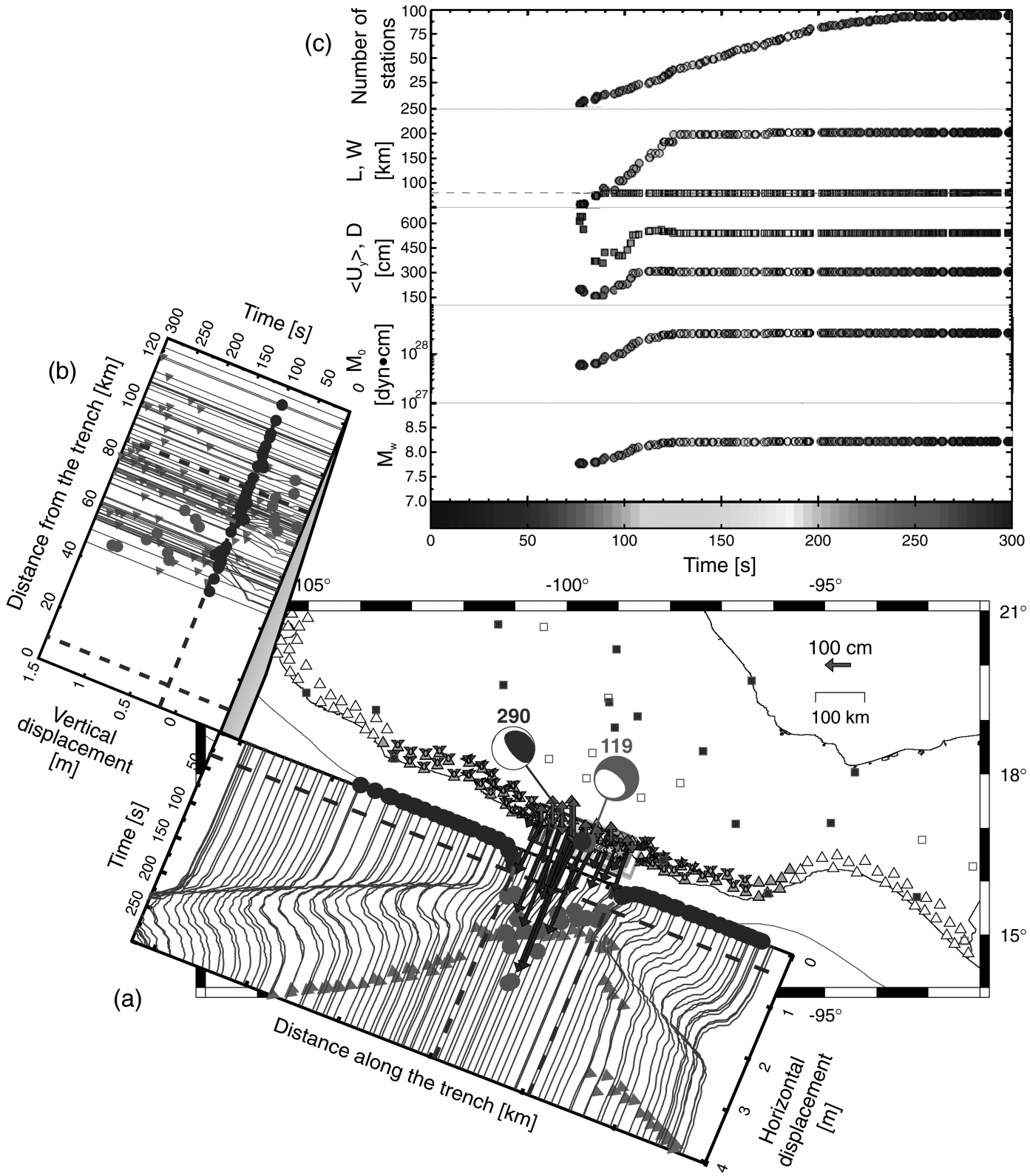

▲ **Figure 4.** Results from test 3. Fault parameters from the proposed GPS station configuration along the coast and focal mechanism from *W*-phase inversion using regional broadband stations. The symbols and panels are the same as for Figure 2.

DISCUSSION AND CONCLUSIONS

The results are encouraging. A sufficiently dense coastal GPS array can certainly provide a first warning in about two minutes and the focal mechanism would be available from the inversion of the regional W-phase in ~5 minutes, which is much less than the 10-minute time frame set forth in the introduction. However, the current configuration of real-time stations along the coast is not enough for a robust and reliable estimation of source parameters for a tsunami warning in Mexico. The large separation between the stations will lead to over-estimation of the fault length, as was the case for the 20 March 2012 event. If all 22 stations that are currently in operation along the Pacific coast had real-time transmission capability, a robust solution for earthquakes $M_w \geq 7.8$ with rupture areas within the Guerrero coast would be possible in less than 5 minutes. Nonetheless, smaller events or those with rupture areas south of station PINO or north of station ZIHP (Fig. 5, Ⓔ supplement) in which the station spacing is larger might be overestimated and may trigger false alerts. Also, it would be impossible to constrain the position of the fault with respect to the coast in these regions, because there is only one row of stations parallel to the coast.

A denser station configuration is proposed, with 120 GPS stations along the coast distributed along two parallel rows with staggered locations. As demonstrated here, with such a network, a robust solution, including M_w and position of the fault, would be available in ~2 min after the origin time. With the dense station distribution and real-time transmission capability, earthquakes with $L \geq 25$ km can be discriminated, reducing the possibility of false alerts produced by small earthquakes.

The precision achievable with a high-rate real-time GPS in a network approach such as ours is of ~1–2 cm in the horizontal and ~5 cm in the vertical (Genrich and Bock, 2006; Bock *et al.*, 2011). However this requires tight baselines such as those proposed in the third test scenario. Current baselines of the GPS network produce displacements precise to ~5 cm in the horizontal and ~10 cm in the vertical (S. I. Franco, personal comm., 2012). However, all SSN GPS stations are collocated with strong-motion instruments and a real-time combination of seismic and GPS data can produce an order of magnitude increase in displacement precision (Bock *et al.*, 2011), which can lead to better detection and modeling of smaller events.

Further tests are needed before full implementation of a tsunami early warning system in Mexico. We have assumed that the event is a shallow-thrust earthquake. Our method would not work if the source is different (i.e., a normal-faulting earthquake in the subducted plate or in the overriding plate).

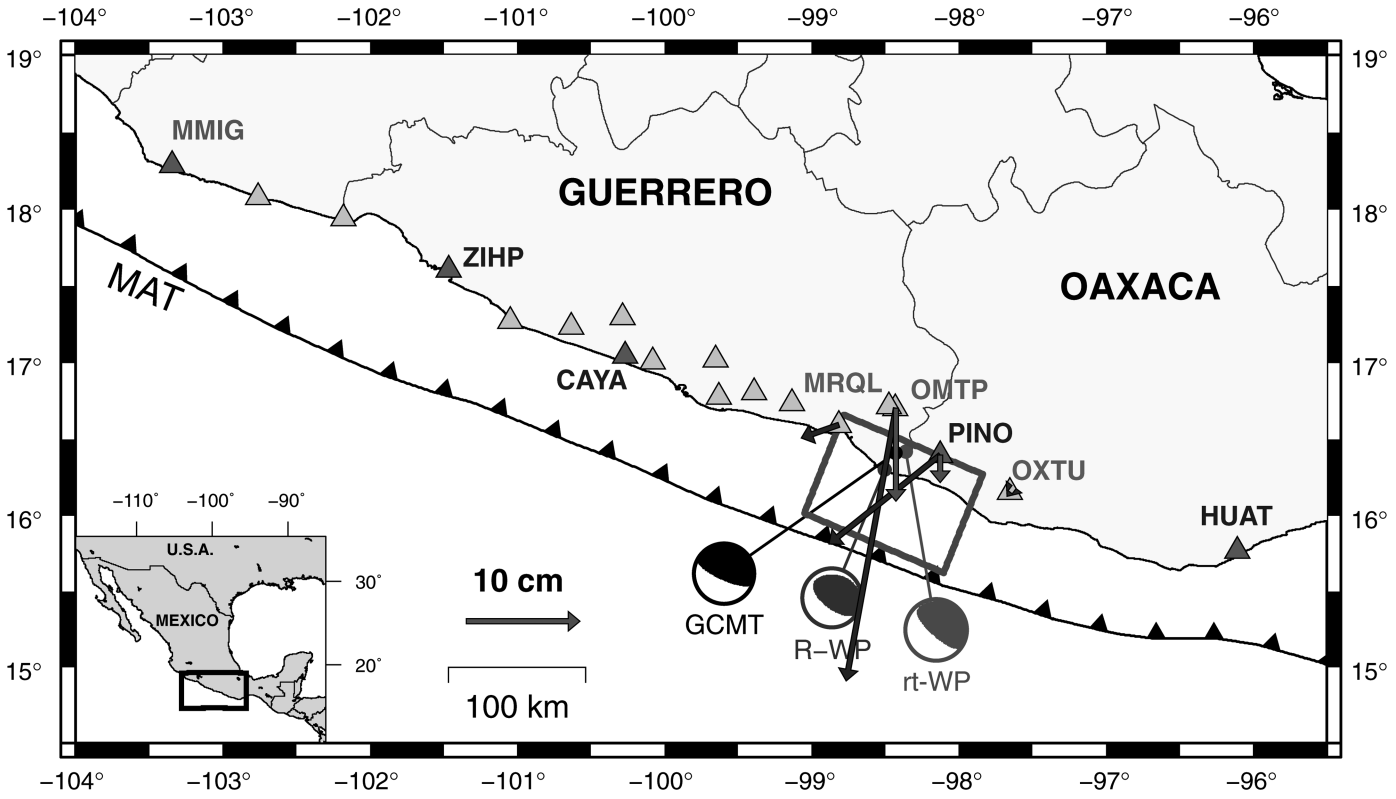

▲ **Figure 5.** Fault parameters for the 20 March 2012 Ometepec earthquake (M_w 7.4). The triangles denote GPS stations: GPS–SSN in dark gray, GPS–IGEF in light gray. The rectangle corresponds to the fault solution. The focal mechanism in light gray corresponds to the real-time solution from W-phase inversion (rt-WP) reported by the SSN; in gray is the revised W-phase inversion (R-WP); in black is the solution reported by Global CMT (GCMT, www.globalcmt.org).

Such events are known to occur near the Mexican coast. In such cases, the static displacement field will differ from that expected from a shallow-thrust event. The algorithm should detect this and proceed directly to the W-phase inversion.

Evidently, estimation of basic-source parameters is a necessary first step but by no means a sufficient one for a near-source tsunami early warning. Once a robust system for magnitude and geometry determination is developed, the next step would be to use these simple source parameters to model the resulting tsunami (Ohta *et al.*, 2012) and broadcast intensity metrics with the warnings. Tsunami modeling can be done by computing the vertical deformation of the crust and forward calculation of the ensuing tsunami. Open-source modeling codes for this are robust and have been benchmarked (e.g., Berger *et al.* (2011)) and could be used to this end.

If the tsunami early warning described in this article is implemented, along with the associated costs in installation and maintenance of the proposed network, it should be accompanied by a comprehensive overhaul of current outreach and education programs for the communities along the coast, as well as protocols for authorities and civil agencies. As discussed by Suárez *et al.* (2009), there is still a substantial divide in Mexico between the scientific and engineering communities that work on design and implementation of early warning and the government and civil society who serve as the user base. A scientific measurement of the size of an earthquake and/or tsunami is only the first part of a collaborative chain between science and the community it serves that needs to be fortified in Mexico.

ACKNOWLEDGMENTS

We thank the G-Gap team and C. DeMets for providing coseismic displacement vectors. PINO, CAYA, and HUAT GPS stations are operated and maintained by SSN. Figures were prepared using Generic Mapping Tools (GMT, Wessel and Smith, 1991). Funding for this work was provided by Conacyt project 82599 and PAPIIT-DGAPA, UNAM project IN114809. XP-C thanks the Tectonics Observatory at Caltech and the Betty and Gordon Moore for partial support during this study.

REFERENCES

Anderson, J. G., S. K. Singh, J. M. Espindola, and J. Yamamoto (1989). Seismic strain release in the Mexican subduction thrust, *Phys. Earth Planet. In.* **58,** 307–322.

Astiz, L., and H. Kanamori (1984). An earthquake soublet in Ometepec, Guerrero, Mexico, *Phys. Earth Planet In.* **34,** 24–25.

Avallone, A., M. Marzario, A. Cirella, A. Piatanesi, A. Rovelli, C. Di Alessandro, E. D'Anastasio, N. D'Agostino, R. Giuliani, and M. Mattone (2011). Very high rate (10 Hz) GPS seismology for moderate-magnitude earthquakes: The case of the M_w 6.3 L'Aquila (central Italy) event, *J. Geophys. Res.* **116,** B02305, doi: 10.1029/2010JB007834.

Berger, M. J., D. L. George, R. J. LeVeque, and K. T. Mandli (2011). The GeoClaw software for depth-averaged flows with adaptive refinement, *Adv. Water Resour.* **34,** 1195–1206.

Bock, Y., D. Melgar, and B. W. Crowell (2011). Real-time strong-motion broadband displacements from collocated GPS and accelerometers, *Bull. Seismol. Soc. Am.* **101,** 2904–2925.

Chael, E., and G. S. Stewart (1981). Recent large earthquakes along the middle America trench and their tectonic implications for the subduction process, *J. Geophys. Res.* **103,** 329–338.

Courboulex, F., M. A. Santoyo, J. F. Pacheco, and S. K. Singh (1997). The 14 September 1995 ($M = 7.3$) Copala, Mexico, earthquake: A source study using teleseismic, regional, and local data, *Bull. Seismol. Soc. Am.* **87,** 999–1010.

Cruz-Atienza, V. M., V. Hjörleifsdóttir, and A. Rocher (2011). Simulando un M 8.2 en la brecha de Guerrero, Reunión Anual 2011, Unión Geofísica Mexicana, *GEOS* **31,** 150.

Cyranosky, D. (2011). Japan faces up to failure of its earthquake preparations, *Nature* **471,** 556–557.

Espinosa-Aranda, J. M., and F. H. Rodríguez (2003). The seismic alert system of Mexico City, in *International Handbook of Earthquake an Engineering Seismology*, Vol. B, International Association of Seismology and Physics of the Earth's Interior, 1253–1259.

Farreras, S. F. (1997). Tsunamis en México, in *Oceanografía Física en México*, M. F. Lavin (Editor), Monografía No. 5, Unión Geofísica Mexicana, Mexico, 73–96.

Genrich, J. F., and Y. Bock (2006). Instantaneous geodetic positioning with 10–50 Hz GPS measurements: Noise characteristics and implications for monitoring networks, *J. Geophys. Res.* **111,** doi: 10.1029/2005JB003617.

Iglesias, A., R. W. Clayton, X. Pérez-Campos, S. K. Singh, J. F. Pacheco, D. García, and C. Valdés-González (2010). *S* wave velocity structure below central Mexico using high-resolution surface wave tomography, *J. Geophys. Res.* **115,** B06307, doi: 10.1029/2009JB006332.

Kanamori, H., P. C. Jennings, S. K. Singh, and L. Astiz (1993). Estimation of strong ground motions in Mexico City expected for large earthquakes in the Guerrero seismic gap, *Bull. Seismol. Soc. Am.* **83,** 811–829.

Mai, P. M., and G. C. Beroza (2002). A spatial random field model to characterize complexity in earthquake slip, *J. Geophys. Res.* **107,** no. B11, 2308, doi: 10.1029/2001JB000588.

Melgar, D., Y. Bock, and B. Crowell (2012). Real-time centroid moment tensor determination for large events from local and regional displacement records, *Geophys. J. Int.* **188,** 703–718.

Nava, A. E. (1984). Estudio de los temblores de Ometepec del 7 de junio de 1982 y sus réplicas, *B. S. Thesis*, Facultad de Ingeniería, Universidad Nacional Autonoma de Mexico.

Nishenko, S. P., and S. K. Singh (1987). The Acapulco–Ometepec, Mexico, earthquakes of 1907–1982: Evidence for a variable recurrence history, *Bull. Seismol. Soc. Am.* **77,** 1359–1367.

Núñez-Cornú, F. J., M. Ortiz, and J. J. Sánchez (2008). The great 1787 Mexican tsunami, *Nat. Hazards* **47,** 569–576, doi: 10.1007/s11069-008-9239-1.

Ohta, Y., T. Kobayashi, H. Tsushima, S. Miura, R. Hino, T. Takasu, H. Fujimoto, T. Iinuma, K. Tachibana, T. Demachi, T. Sato, M. Ohzono, and N. Umino (2012). Quasi real-time fault model estimation for near-field tsunami forecasting based on RTK-GPS analysis: Application to the 2011 Tohoku–Oki earthquake (M_w 9.0), *J. Geophys. Res.* **117,** doi: 10.1029/2011JB008750.

Okada, Y. (1992). Internal deformation due to shear and tensile faults in a half space, *Bull. Seismol. Soc. Am.* **82,** 1018–1040.

Olsen, K. B., S. M. Day, L. A. Dalguer, J. Mayhew, Y. Cui, J. Zhu, V. M. Cruz-Atienza, D. Roten, P. Maechling, T. H. Jordan, D. Okaya, and A. Chourasia (2009). ShakeOut-D: Ground motion estimates using an ensemble of large earthquakes on the southern San Andreas fault with spontaneous rupture propagation, *Geophys. Res. Lett.* **36,** L04303, doi: 10.1029/2008GL036832.

Ordaz, M., J. Arboleda, and S. K. Singh (1995). A scheme of random summation of an empirical Green's function to estimate ground motions from future large earthquakes, *Bull. Seismol. Soc. Am.* **85,** 1635–1647.

Ozaki, T. (2011). Outline of the 2011 off the Pacific coast of Tohoku Earthquake (M_w 9.0)—Tsunami warnings/advisories and observations, *Earth Planets Space* **63,** 827–830.
Pacheco, J. F., and S. K. Singh (2010). Seismicity and state of stress in Guerrero segment of the Mexican subduction zone, *J. Geophys. Res.* **115,** B01303, doi: 1029/2009JB006453.
Pérez-Campos, X., Y. Kim, A. Husker, P. M. Davis, R. W. Clayton, A. Iglesias, J. P. Pacheco, S. K. Singh, V. C. Manea, and M. Gurnis (2008). Horizontal subduction and truncation of the Cocos Plate beneath central Mexico, *Geophys. Res. Lett.* **35,** L18303, doi: 10.1029/2008GL035127.
Quintanar, L. (1985). Variaciones espacio-temporales de la sismicidad en la reión costera de Oaxaca de 1950 a 1982 (mb > 4.3), *Master's Thesis*, Facultad de Ciencias, Universidad Nacional Autónoma de México, México, D. F., México.
Rivera, L., H. Kanamori, and Z. Duputel (2011). *W* phase source inversion using the high-rate regional GPS data of the 2011 Tohoku-Oki earthquake, *American Geophysical Union*, Abstract G33C-04.
Sánchez, A. J., and S. F. Farreras (1993). *Catalog of Tsunamis on the Western Coast of Mexico*, World Data Center A for Solid Earth Geophysics, Publication SE-5O, National Geophysical Data Center, NOAA, Boulder, Colorado, U.S.A., 79 pp.
Singh, S. K., and F. Mortera (1991). Source time functions of large Mexican subduction earthquakes, morphology of the Benioff zone, age of the plate and their tectonic implications, *J. Geophys. Res.* **96,** 21,487–21,502.
Singh, S. K., L. Astiz, and J. Havskov (1981). Seismic gaps and recurrence periods of large earthquakes along the Mexican subduction zone: A reexamination, *Bull. Seismol. Soc. Am.* **71,** 827–843.
Singh, S. K., J. M. Espinosa, J. Yamamoto, and J. Havskov (1982). Seismic potential of the Acapulco-San Marcos region along the Mexican subduction zone, *Geophys. Res. Lett.* **9,** 633–636.
Singh, S. K., X. Pérez-Campos, A. Iglesias, and D. Melgar (2012). A method for rapid estimation of moment magnitude for early tsunami warning based on coastal GPS networks, *Seismol. Res. Lett.* **83,** 517–531.
Singh, S. K., X. Pérez-Campos, A. Iglesias, and J. F. Pacheco (2008). An exploratory study for rapid estimation of critical source parameters of great subduction-zone earthquakes in Mexico, *Geofisc. Int.* **47,** 355–369.
Singh, S. K., L. Ponce, and S. P. Nishenko (1985). The great Jalisco, Mexico, earthquakes of 1932: Subduction of the Rivera plate, *Bull. Seismol. Soc. Am.* **75,** 1301–1313.
Singh, S. K., G. Suárez, and T. Domínguez (1985). The Oaxaca, Mexico earthquake of 1931: Lithospheric normal faulting in the subducted Cocos plate, *Nature* **137,** 56–58.
Singh, S. K., J. Yamamoto, J. Havskov, M. Guzmán, D. Novelo, and R. Castro (1980). Seismic gap of Michoacan, Mexico, *Geophys. Res. Lett.* **7,** 69–72.
Smalley, R. (2009). High-rate GPS: How high do we need to go? *Seismol. Res. Lett.* **80,** 1054–1061.
Suárez, G., and P. Albini (2009). Evidence for great tsunamigenic earthquakes (*M* 8.6) along the Mexican subduction zone, *Bull. Seismol. Soc. Am.* **99,** 892–896.
Suárez, G., T. Monfret, G. Wittlinger, and C. David (1990). Geometry of subduction and depth of the seismogenic zone in the Guerrero Gap, Mexico, *Nature* **345,** 336–338.
Suárez, G., D. Novelo, and E. Mansilla (2009). Performance evaluation of the seismic alert system (SAS) in Mexico City: A seismological and a social perspective, *Seismol. Res. Lett.* **80,** 707–726.
Tinti, E., E. Fukuyama, A. Piatanesi, and M. Cocco (2005). A kinematic source-time function compatible with earthquake dynamics, *Bull. Seismol. Soc. Am.* **95,** 1211–1223, doi: 10.1785/0120040177.
UNAM Seismology Group (1986). The September 1985 Michoacan earthquakes: Aftershock distribution and history of rupture, *Geophys. Res. Lett.* **13,** 573–576.
UNAM Seismology Group (2013). Ometepec-Pinotepa, Mexico earthquake of 20 March 2012 (M_w 7.5): A preliminary report, *Geofisc. Int.* **52,** no. 2 (in press).
Wessel, P., and W. H. F. Smith (1991). Free software helps map and display data, *Eos Trans. AGU* **72,** no. 441, 445–446.
Yoffe, E. (1951). The moving Griffith crack, *Phil. Mag.* **42,** 739–750.

Xyoli Pérez-Campos
Shri K. Singh
Víctor Cruz-Atienza
Arturo Iglesias
Vala Hjörleifsdóttir
Departamento de Sismología
Instituto de Geofísica
Universidad Nacional Autónoma de México
Circuito de la Investigación s/n
Ciudad Universitaria
Coyoacán, México, D. F. 04400, Mexico
xyoli@geofisica.unam.mx

Diego Melgar
Institute of Geophysics and Planetary Physics
Scripps Institution of Oceanography
University of California, San Diego
9500 Gilman Drive
La Jolla, California 92093-0225 U.S.A.